Size and polydispersity effect on the magnetization of densely packed magnetic nanoparticles.

Vincent Russier, Caroline de Montferrand, Yoann Lalatonne, Laurence Motte

Size and polydispersity effect on the magnetization of densely packed magnetic nanoparticles.

Vincent Russier [a)], Caroline de Montferrand [b)], Yoann Lalatonne [b)] and Laurence Motte [b)]

[a)] *ICMPE, UMR 7182 CNRS and UPEC,*

2-8 rue Henri Dunant 94320 Thiais, France,

[b)] *CSPBAT UMR 7244 CNRS and University Paris 13, 93017 Bobigny, France.*

The magnetic properties of densely packed magnetic nanoparticles (MNP) assemblies are investigated from Monte Carlo simulations. The case of iron oxide nanoparticles is considered as a typical example of MNP. The main focus is put on particle size and size polydispersity influences on the magnetization curve. The particles are modeled as uniformly magnetized spheres isolated one from each other by a non magnetic layer representing the organic coating. A comparison with recent experimental results on $\gamma-Fe_2O_3$ powder samples differing by their size is given.

I. INTRODUCTION

The physics and chemistry of nanoscale magnetic particles (MNP) still gives rise to an important research activity due both to their wide range of potential applications and their own fundamental interest [1–4]. Among the large variety of MNP, iron oxide based ones $\gamma-Fe_2O_3$ and Fe_3O_4 take a particular place in the field of biological and medical applications because of their bio-compatibility and suitable superparamagnetic properties. To translate intrinsic properties of nanoparticles to various applications, there is a need to control nanoparticle dispersions. Consequently nanoparticles are usually coated by an organic surfactant [5, 6] in order to prevent aggregation. The influence of this non magnetic layer and then the nanoparticles contact distance play a major role on collective magnetic properties [7]. A complete understanding of the macroscopic magnetic properties of MNP assemblies in terms of their individual intrinsic characteristics on the one hand and of the size distribution and volume concentration on the other hand is of crucial importance. Indeed this is a mean to get informations on the relevant parameters of the distribution and MNP properties from the magnetic measurements. Two key features which strongly influence the macroscopic magnetic properties of these systems are the magnetic structure at the particle scale, where core shell structure and spin canting effect can be invoked [8–11] and the size distribution generally described through a lognormal law for the diameters distribution.

At temperatures higher than the blocking temperature T_b where the MNP are in the superparamagnetic regime [1, 4] and in case of weak interparticle interactions, namely for both small particles concentrations and in the absence of cluster formation the physical properties of MNP assemblies are well understood. The magnetization curve, $M(H)$ of the whole assembly follows then a Langevin like function weighted by the diameter distribution function and eventually modified in order to take into account a core-shell structure [12–14]. Moreover the one-body magnetocrystaline anisotropy energy of the MNP can also be taken into account and this modifies the $M(H)$ curve from the original Langevin function [15, 16]. The core shell structure of the MNP may consist simply of the inclusion of a magnetic dead layer at the surface of the MNP [10, 11] or of the introduction of an additional paramagnetic component in the MNP [14]. The symmetry breaking at the surface can lead to surface effects on the anisotropy energy of each MNP with noticeable effects on the $M(H)$ curve [17–19] . In case of diluted assemblies of spherical MNP when the particles are non or weakly interacting, the non interacting particles type of approach of the magnetization curve leads to a reasonable determination of the characteristics of the individual particles and of the size distribution namely the median diameter d_m and the $\ln(d)$ standard deviation σ. However, when the NP concentration increases, the interparticles interactions must be taken into account. These ones which for spherical and well coated MNP include mainly the interactions between the

MNP magnetic dipoles (DDI), have been widely studied and a large amount of works and methods are thus available going from mean field approximation, thermodynamic perturbation theory (TPT) [18, 20] for weakly interacting systems to numerical simulations for moderate to strongly interacting systems [18, 21, 22]. The mean field and TPT provide an illustrative physical picture of the relation between the local structure and either the magnetization in terms of the applied field or the susceptibility. For instance the demagnetizing field effect depending on the external shape of the system, is well reproduced by the TPT [20]. As a link between TPT and numerical simulations, the description based on the interaction fields distributions [23] which explains the DDI induced reduction of the magnetization of an isotropic system as a generalization of a similar result obtained using the TPT and suggests that the DDI induced reduction of the magnetization is not related to an antiferromagnetic behavior. However, for strongly interacting systems, as in lyophilized powder samples or high concentration MNP assemblies embedded in a non magnetic matrix the numerical simulations seem more adapted. Although numerical simulations of magnetic properties of MNP assemblies are now many, a systematic study of the mean size and polydispersity effects especially for randomly organized particles with high concentration is still missing.

The aim of this work is to investigate this problem and to interpret recent experimental measurements [24] on powder samples of maghemite MNP assemblies differing by their median size. We present a Monte Carlo (MC) simulation of the mean particle size and polydispersity effect on the DDI in random and densely packed spherical clusters of coated spherical maghemite MNP. Our main purpose is to model the case of lyophilized powders or high concentration of particles embedded in a non magnetic matrix. A particular attention is paid to the linear susceptibility χ, and its dependence on the median size of the size distribution. It is found that χ as a function of d_m may present a plateau, leading to a quasi independence of the magnetization with respect to d_m in the vicinity of the low external fields. The magneto crystalline anisotropy is then shown to play a role for larger values of the field when the particles remain in the superparamagnetic regime in agreement with the findings of Ref. [15, 25] for non interacting particles, in the TPT regime [20] and in preceding MC simulations [18, 22, 26]. As an application, we focus on the experimental magnetization curves of Ref. [24].

II. MODEL FOR DENSELY PACKED ASSEMBLIES

The model we use is designed to simulate the properties of either lyophilized powders samples or high concentration nanoparticles assemblies embedded in non magnetic matrix. As is usually done to model single domain MNP, the nanoparticles are modeled as non overlapping spheres bearing at their center a permanent point dipole representing the uniform magnetization of the particle

(super spin). The moment of each particle is equal to its volume times the bulk magnetization, M_s, which means that neither spin canting effect nor magnetic dead layer at the particle surface is considered. We also include the magneto crystalline anisotropy with the same anisotropy constant K_1 on all particles. The particles are supposed to be coated by a non magnetic layer of thickness $\Delta/2$, representing the usual coating by organic surfactant molecules. The layer thickness is taken as $\Delta/2$ for convenience (see below). The particle diameters, $\{d_i\}$ are distributed according to a log-normal law defined by the median diameter d_m and the standard deviation σ of $ln(d)$,

$$f(d) = \frac{1}{d\sqrt{2\pi}\sigma} \exp\left(-\frac{(\ln(d/d_m))^2}{2\sigma^2}\right) \tag{1}$$

d_m and σ are related to the mean diameter and the diameter standard deviation σ_d through $d_1 = d_m e^{\sigma^2/2}$ and $\sigma_d = d_m\sqrt{(e^{\sigma^2}-1)e^{\sigma^2}}$. In the following, we use d_m as the unit of length, and thus in reduced unit, the distribution function is totally determined by the single parameter σ which characterizes the system polydispersity.

We consider mainly spherical clusters, where owing to the global shape isotropy the demagnetizing effects vanish, with free boundary conditions. This choice of large spherical clusters can be justified on the experimental point of view since upon drying the NP are likely to aggregate in spherical shaped large clusters which has been confirmed from simulations [5]. Our first purpose is to focus on the contribution of the dipolar interactions (DDI) to the magnetization curve, especially in the moderate to strong coupling regime when particles surrounded by their coating layer are at contact. The geometrical configuration of two particles of different sizes at contact with their coating layer is displayed in figure (1). Moreover, we consider temperatures such that the particles of size d_m are superparamagnetic; as we shall see later for polydisperse systems due to the presence of large particles in the distribution, this condition may not be strictly fulfilled. When taken into account the magnetocrystalline anisotropy is considered in its simplest form, namely in the uniaxial symmetry and at lowest order [2, 4]. The total energy thus includes the DDI, the one-body anisotropy term and the Zeeman term corresponding to the interaction with the external applied field $\vec{H}_a = H_a\hat{h}$. Let $\{\vec{r}_i\}$, $\{v(i)\}$, $\{\vec{m}_i\}$ and $\{\vec{n}_i\}$ denote the particles locations, volumes, moments and easy axes respectively. The total energy of the cluster reads

$$E = \frac{\mu_0}{4\pi} \sum_{i<j} m_i m_j \frac{\hat{m}_i\hat{m}_j - 3(\hat{m}_i\hat{r}_{ij})(\hat{m}_j\hat{r}_{ij})}{r_{ij}^3} - K_1 \sum_i v(i)(\hat{n}_i\hat{m}_i)^2 - \mu_0 H_a \sum_i m_i\hat{m}_i\hat{h} \tag{2}$$

where hated letters denote unit vectors, m_i are the moment magnitudes, $r_{ij} = |\vec{r}_i - \vec{r}_j|$. It is worth mentioning that the consideration of the anisotropy term with a fixed easy axes distribution means that the magnetization relax according to a Néel process [27, 28], namely the particles are

considered fixed while their moment relaxes relative to their easy axis. In this work only the case of a random distribution of easy axes is considered. In the following we use reduced quantities; first the energy is written in $k_B T_0$ units, T_0 being a suitable temperature ($T_0 = 300K$ in the present work) and we introduce a reference diameter, d_{ref}. The reference diameter, d_{ref} is a length unit independent of the size distribution, useful for the energy couplings, and can be chosen from a convenient criterion independently of the actual structure of the MNP assembly. The reduced total energy is given by

$$
\begin{aligned}
\beta_0 E &= -\epsilon_K^{(0)} \left(\frac{d_m}{d_{ref}}\right)^3 \sum_i d_i^{*3} (\hat{n}_i \hat{m}_i)^2 - \epsilon_d^{(0)} \left(\frac{d_m}{d_{ref}}\right)^3 \sum_{i<j} d_i^{*3} d_j^{*3} \frac{\hat{m}_i \hat{m}_j - 3(\hat{m}_i \hat{r}_{ij})(\hat{m}_j \hat{r}_{ij})}{r_{ij}^{*3}} \\
&\quad - h \sum_i d_i^{*3} \hat{m}_i \hat{h} \\
\epsilon_d^{(0)} &= \frac{\beta_0 \mu_0}{4\pi} (\pi/6)^2 M_s^2 d_{ref}^3 \quad \epsilon_K^{(0)} = \beta_0 K_1 v(d_{ref}) \\
h &= \beta_0 \mu_0 M_s (\pi/6) d_m^3 H_a \equiv \left(\frac{d_m}{d_{ref}}\right)^3 \frac{H_a}{H_{ref}}
\end{aligned}
\tag{3}
$$

where $\beta_0 = (k_B T_0)^{-1}$ and the stared lengths are in d_m unit. The dimensionless dipolar coupling constant and anisotropy constant are then $\epsilon_d = (d_m/d_{ref})^3 \epsilon_d^{(0)}$ and $\epsilon_K = (d_m/d_{ref})^3 \epsilon_K^{(0)}$ respectively; the reference diameter, d_{ref} can be chosen such that $\epsilon_d(d_m = d_{ref}) \equiv \epsilon_d^{(0)} = 1$; the reduced external field h coincides with the usual Langevin variable at temperature T_0 for a monodisperse distribution with $d = d_m$ In equation (3), we also introduce the reference external field, H_{ref} for convenience.

Concerning the structure in position, the nanoparticles surrounded by their coating layer Δ form an assembly of hard spheres of effective diameters $\{d_i + \Delta\}$ (see figure (1)) which are arranged in large densely packed clusters with either a random or a well ordered structure (simple cubic or face centered cubic lattice). We build these clusters in two steps. First a large stacking of the coated spheres is made in a parallepipedic box with the desired structure, random or well ordered. In the random case, this first step is made from a sequential random rain plus compression algorithm in such a way to maximize the packing fraction. Doing this we can get a packing fraction φ for the effective spheres corresponding to the so-called loose random packing [29] ($\varphi \simeq 0.60$ in the monodisperse case). Once this first step is performed, we cut within the global stacking the cluster we want to study by imposing both the external shape, either spherical or prismatic, and the number of particles N_p, with typically $N_p \simeq 1000$. The central part of some of the clusters used in the present work corresponding to different values of the polydispersity, σ is shown in figure (2) to illustrate the structures obtained. It is important to note that because of the coating layer of thickness $\Delta/2$ the closest distance of approach between particles i, j is shifted from $(d_i + d_j)/2$ to

$(d_i + d_j)/2 + \Delta$ and as a result the sum involved in equation (3) depends on the actual magnetic particles concentration of the cluster through the value chosen for Δ. One can rewrite the DDI sum by using another length scale, namely $(d_m + \Delta)$ in order to exhibit a contribution independent of Δ. Doing this, the total DDI energy reads

$$\epsilon_d^{(0)} \left(\frac{d_m}{d_{ref}}\right)^3 \left(\frac{d_m}{d_m + \Delta}\right)^3 \sum_{i<j} d_i^{*3} d_j^{*3} \frac{\hat{m}_i \hat{m}_j - 3(\hat{m}_i \hat{r}_{ij})(\hat{m}_j \hat{r}_{ij})}{(r_{ij}/(d_m + \Delta))^3} \tag{4}$$

We recall that the distribution of reduced diameters, $\{d_i^*\}$ depends only on the value of σ, which is conserved through a scaling operation corresponding to a change of d_m. The sum of equation (4) is a geometric sum characteristic of the DDI expected, at least for small values of σ, to be independent of Δ and thus to characterize the reduced DDI sum of the most concentrated cluster ($\Delta = 0$) of the structure (s.c., f.c.c., random) considered. In other words, equation (4) allows to explicit the dependence of the dipolar coupling with respect to the particles volume fraction, φ_v. For this we note that $(d_m/(d_m + \Delta))^3$ can be rewritten as φ_v/φ_m where φ_m ($\equiv \varphi_v(\Delta = 0)$) is the maximum value of φ_v for the given configuration, namely the volumic fraction corresponding to the spheres of diameters $\{d_i + \Delta\}$. $\varphi_m = \pi/6$, 0.74, and ~ 0.60 for the simple cubic, fcc and the loose random packed structures respectively. Then from (4), we can introduce an effective dipolar coupling constant, say $\epsilon_d^{(eff)} = \epsilon_d^{(0)}(d_m/d_{ref})^3(d_m/(d_m + \Delta))^3$ which is rewritten as $\epsilon_d^{(eff)} = (\varphi_v/\varphi_m)(d_m/d_{ref})^3$, since $\epsilon_d^{(0)}=1.0$. Now, one can replace both d_m and Δ by say d_{m2} and Δ_2 respectively in such a way that the total DDI energy remains constant by imposing

$$\left(\frac{d_m}{d_{ref}}\right)\left(\frac{d_m}{d_m + \Delta}\right) = \left(\frac{d_{m2}}{d_{ref}}\right)\left(\frac{d_{m2}}{d_{m2} + \Delta_2}\right) \tag{5}$$

leading to

$$d_{m2} = \frac{d_m}{2(1 + \Delta/d_m)} \left\{ 1 + \left[1 + 4\frac{\Delta_2}{d_m}\left(1 + \frac{\Delta}{d_m}\right)\right]^{1/2} \right\} \tag{6}$$

In the absence of anisotropy energy, namely when only the DDI is taken into account, the two systems characterized by (d_m, Δ) and (d_{m2}, Δ_2) are similar and therefore present the same magnetization curve in terms of the reduced field h. Furthermore this holds also whatever the value of ϵ_K in the vicinity of zero external field because for random distribution of easy axes the linear susceptibility χ does not depend on ϵ_K in the superparamagnetic regime. Doing the transformation (6), the actual values of $\{\vec{r}_i\}$ are scaled according to the value of $(d_m + \Delta)$. Our hypothesis of a value of σ for the reduced diameter distribution to be not (or only negligibly) modified holds rigorously in the quasi monodisperse case ($\sigma << 1$). Consequently we shall use in the following

the scaling transformation (6) only in quasi monodisperse situations.

In the present work we focus on both the reduced magnetization per unit magnetic volume in the direction of the external applied field,

$$M_r = \frac{M(h)}{M_s} = \frac{< \sum_i v(i) \hat{m}_i \hat{h} >}{\sum_i v(i)} \qquad (7)$$

and the linear susceptibility,

$$\chi = \frac{\partial M}{\partial H} = \frac{M_s}{H_{ref}} \left(\frac{d_m}{d_{ref}} \right)^3 \frac{\partial M_r}{\partial h} = \frac{M_s}{H_{ref}} \left(\frac{d_m}{d_{ref}} \right)^3 \chi_r \qquad \text{with} \qquad \chi_r = \frac{\partial M_r(h)}{\partial h} \qquad (8)$$

where we have used equation (3) to introduce the reduced susceptibility, χ_r. The susceptibility can also be obtained from the fluctuations :

$$\chi_r = \beta^* \sum_i \frac{v(i)}{v(d_m)} \left(\frac{< \left(\sum_i v(i) \hat{m}_i \hat{h} \right)^2 >}{(\sum_i v(i))^2} - M_r^2 \right). \qquad (9)$$

As a rule, we use this second way with the direct derivative merely used as a check of the calculation.

When the anisotropy energy is zero, the magnetization curve can be simulated either starting from $h = 0$ and increasing the field step by step or from the starurated situation, and decreasing h down to $h = 0$. When the anisotropy energy is included and since we may get an opening of the hysteresis loop, we start from the saturated case at sufficiently high applied field, and decrease the field beyond $-h_{irr}$ where the irreversible field h_{irr} is defined as the value of h below which the hysteresis cycle opens. In cases where the hysteresis cycle opens, we also define an anhysteretic magnetization curve from the downward and the upward magnetization curves which because of the symmetry of our system reads

$$M_r^{(an)}(h) = \frac{1}{2}(M_r^{(d)}(h) + M_r^{(u)}(h)) = \frac{1}{2}(M_r^{(d)}(h) - M_r^{(d)}(-h)) \qquad (10)$$

The magnetization curves $M(h)$ in terms of the external field are determined from Monte Carlo simulations, by fixing the locations of the particles in the cluster. We consider free boundary conditions, and the clusters includes ca 1000 particles. The dipolar coupling parameter is determined from equation (3). In section III C we consider a given set of experimental results in order to illustrate the model; nevertheless we do not restrict this latter only to this well specified set of samples but instead use the characteristics of maghemite as typical example for MNP assemblies. For the bulk magnetization M_s we use a commonly accepted value for maghemite. Using M_s varying from 80 to 84 emu/g, or $\sim$ 75.0 emu/g, if we take into account the temperature dependence, and ρ

$= 4.870 \text{g/cm}^3$ leads to $\mu_0 M_s$ from 0.459 T to 0.514 T; at $T_0 = 300$K we get $\epsilon_d^{(0)} = 1.0$ for d_{ref} varying from 9.665 nm to 10.422 nm and we use in the following except otherwise mentioned d_{ref} = 10 nm which corresponds to $\mu_0 M_s = 0.488$T and $H_{ref} = 16.20$ kA/m. The anisotropy constant K_1 cannot be taken equal to the bulk effective magnetocrystalline anisotropy constant K_b as it is found to be much larger when the particle size decreases. A rather wide spectrum of values can be found in the literature for K_1, corresponding to (K_1/K_b) lying in between ~ 4 to 15 for particle diameters of ca 12 nm or smaller [30–34]. In the following we use either $(K_1/K_b) \simeq 4$ or 2, since we consider particles with mean diameters larger than 10 nm. With $K_b = 0.47 \ 10^4 \ J/m^3$ [10, 31] this leads to $\epsilon_K^{(0)} = 2.38$ and 1.19 respectively. In any case, both M_s and K_1 are to be understood merely as realistic instead of truly accurate experimental values given the simplicity of the model.

Our Monte Carlo simulations are based on the usual Metropolis scheme [35, 36]; the averages are taken over 10 to 40 independent runs each of which consists in 10^4 to 2.10^4 MC steps (MCS) of equilibration followed by 2.10^4 to 3.10^4 MCS for the averages calculations. Each MCS consists in one trial move per moment in average. The trial move on the unit moment $\hat{m}_i$ consists in moving $\hat{m}_i$ to $(\hat{m}_i + w\vec{u})/|\hat{m}_i + w\vec{u}|$ where $\vec{u}$ is a random vector picked within the unit sphere with uniform probability density. This remains to move $\hat{m}_i$ in a cone of maximum deviation $\delta\theta$ whose value is controlled by the amplitude parameter, w. For $\delta\theta << 1$, we have $\delta\theta \simeq w$. The value of w can be either fixed for a time scale mapping of the MCS or determined in a self consistent way in order to optimize the sampling by imposing a value for the acceptance ratio, R. The former version of this scheme corresponds to the time quantified Monte Carlo algorithm (TQMC) [37, 38] in its first formulation ignoring the precessional step [37]. In the absence of anisotropy energy, the time scale mapping is irrelevant for the present purpose since we expect neither a ferromagnetic behavior nor a metastable blocked regime. Thus in this case, w is self consistently determined in such a way that $R = 0.5$. Conversely, when $\epsilon_K^{(0)} \neq 0$, especially for polydisperse distributions we expect the largest particles to be in blocked state leading to a remanent state all the more that the DDI increase the blocking temperature. Hence, especially in the vicinity of $h = 0$, we deal with a metastable state whose life time must be comparable to the long scale measuring time τ_m. Strictly speaking one has to perform MC simulations corresponding to τ_m and to use the version of the scheme outlined above allowing a mapping of the MC step on the true relaxing time. Since we are interested only in the long time behavior (corresponding to the SQUID measurements time scale), we do not focus on a precise mapping of the MCS scaling time. Instead, we determine w from the behavior of the instantaneous polarization $M(t)$, versus t in MCS along a MC run at $h = 0$ starting from $\{\hat{m}_i\} = \hat{z}$. In other words, we chose w in order to avoid nonphysical jumps over the anisotropy energy barrier. By varying w we get as expected a w dependent evolution of

$M(t)$ before reaching a fluctuating behavior around a well defined plateau; the long time mean value $< M(t) >$ determined beyond some threshold t value and for t up to 2.10^5 MCS is found independent of w at least for w varying in the range $w = 0.03$ to 0.25 for typical values of the parameters we consider ($\epsilon_d \simeq 2$ to 8, $\epsilon_K^{(0)} \simeq 2.3$) and the polydispersity deviation $\sigma = 0.28$. Therefore, in the following, we fix $w = 0.25$ when $\epsilon_K^{(0)} \neq 0$.

III. RESULTS AND DISCUSSION

A. Weak coupling case

Before focusing on the powder like situation characterized by a moderate to strong dipolar coupling, we consider the weak coupling limit of the DDI, $\epsilon_d < 1$ with $\epsilon_K = 0$ where one can compare the results to the analytical one obtained from the thermodynamic perturbation theory and make the link with the mean field approximation. The important point is that one can deduce at least qualitatively when ϵ_d deviates from the limit $\epsilon_d << 1$, the general behavior of the magnetization with respect to the DDI. In this framework, we can expand both the magnetization $M_r(h)$ and the susceptibility χ_r in terms of ϵ_d [18, 20].

$$M_r(h) = M_r^{(0)}(h) + M_r^{(1)}(h)\epsilon_d + \frac{1}{2}M_r^{(2)}\epsilon_d^2$$
$$\chi_r = \chi_r^{(0)} + \chi_r^{(1)}\epsilon_d + \frac{1}{2}\chi_r^{(2)}\epsilon_d^2 \tag{11}$$

$M_r^{(0)}$ and $\chi_r^{(0)}$ correspond to the non interacting case, namely

$$M_r^{(0)}(h) = \frac{\int v(d)L(\beta^*(d/d_m)^3 h)f(d)d(d)}{\int v(d)f(d)d(d)} \tag{12}$$

where L is the Langevin function; $\chi_r^{(0)}$ is directly related to $M_r^{(0)}(h)$ and at $h = 0$ leads to the linear susceptibility of the non interacting system

$$\chi_r^{(0)}(0) = \beta^*(d_6^*/d_3^*)/3 = \beta^* \exp(27\sigma^2/2)/3 \tag{13}$$

where d_s^* is the s-th reduced moment of the distribution $f(d)$. Equation (13) explicits the effect of the polydispersity through the factor (d_6^*/d_3^*), written here in terms of σ for the lognormal distribution. The expansions (11) which have been explicited in the framework of the TPT in [20, 26] depend on geometrical sums which can be directly calculated from the structure considered. More-

over, the linear part with respect to h of $M_r^{(1)}(h)$ can be deduced in the mean field approximation of the magnetization which introduces the DDI contribution to M_r from the demagnetizing field and follows from $M_r(H_a) = M_r^{(0)}(H_{eff})$ where $M_r^{(0)}$ corresponds to the non interacting system and H_{eff} is the effective field

$$H_{eff} = H_a - (D_\alpha - 1/3)M_v^{(0)}(H_a) \; ; \tag{14}$$

D_α is the demagnetizing factor of the sample in the direction of the external field, $\hat{h} = e_\alpha$, and M_v is the total magnetization per unit volume which is related to either the number of MNP per unit volume, ρ, or the MNP volumic fraction, φ_v, through

$$M_v^{(0)} = M_s M_r^{(0)}(H_a)\rho \int v(d)f(d) = M_s M_r^{(0)}(H_a)\varphi_v \tag{15}$$

Using equation (12) for $M_r^{(0)}$ and keeping only the first order term with respect to h, we get

$$H_{eff} = H_a - \frac{1}{3}(D_\alpha - 1/3)M_s\beta^* \frac{d_6^*}{d_3^*}h \tag{16}$$

which is then inserted in the mean field expression for $M_r(H_a)$; then form an expansion of $M_r^{(0)}$ at first order with respect to h and from equation (3) for ϵ_d, we get

$$M_r^{(1)}(h) = -\beta^{*2}(D_\alpha - 1/3)\frac{8}{3}\varphi_v \left(\frac{d_6^*}{d_3^*}\right)^2 h \tag{17}$$

Equation (17) can be equivalently rewritten, in terms of $\Delta M_r = M_r(\epsilon_d) - M_r(\epsilon_d = 0)$, as

$$\frac{\partial(\Delta M_r(h))}{\partial\epsilon_d} = -\beta^{*2}(D_\alpha - 1/3)\frac{8}{3}\varphi_v \left(\frac{d_6^*}{d_3^*}\right)^2 h$$

$$and \; C_2 = \frac{\partial^2 \Delta M_r(h)}{\partial\epsilon_d \partial h}(h = 0, \epsilon_d = 0) \equiv \frac{\partial\chi_r}{\partial\epsilon_d} = -\beta^{*2}(D_\alpha - 1/3)\frac{8}{3}\varphi_v \left(\frac{d_6^*}{d_3^*}\right)^2 \tag{18}$$

A result in agreement with refs. [20] and [26] in the monodisperse case. Here, the important point is that we explicitly write down the effect of the polydispersity through the factor $(d_6^*/d_3^*)^2$ which strongly deviates from unity once σ takes non negligible values. It is worth mentioning that the preceding equations hold when either $\epsilon_d << 1$ or $\varphi_v << 1$. We have performed MC simulations of the magnetization at small values of the coupling constant for prismatic clusters corresponding to either well ordered (simple cubic, and c.f.c) or random structures with a monodisperse particles distribution, and a random structure with a polydispersity characterized by $\sigma = 0.28$. The results

for the second derivative of ΔM_r with respect to ϵ_d and h, C_2, is displayed in table I. As can be seen, especially for $\hat{h} = \hat{z}$, the mean field approximation or equivalently the linear contribution of the TPT compares well with the MC simulations and in particular for the polydispersity effect.

Since spherical or cubic systems are characterized by $D_\alpha = 1/3$, this first term vanishes in these situations and one is left for the DDI contribution with $\Delta M_r \propto \epsilon_d^2$ and similarly for χ_r. Moreover, still for isotropic systems, we know that the DDI contribution to both M_r and χ is negative. Therefore the magnetization is all the more reduced due to the DDI that the coupling constant ϵ_d increases. From the analytical results of the TPT we can calculate the proportionality coefficient relating $(\chi_r(\epsilon_d) - \chi_r(0))$ to ϵ_d^2. We have thus compared the MC simulation to the theoretical small ϵ_d expansion in the simple cubic structure case and a monodisperse distribution. From this comparison, see figure 3, we can check that the TPT gives an accurate result only for $\epsilon_d < 0.2$ as expected. Furthermore, from a description based on the dipolar fields distributions which can be seen as a generalization of the mean field type of approach, ref. [23] have shown also that the dipolar interactions in isotropic systems decrease the magnetization. This decreases is related to the non linearity with respect to the applied field of the non interacting contribution $\chi_r^{(0)}$ to the susceptibility. Notice that this second type of approach, which remains qualitative in the absence of a theory to deduce the dipolar field distribution, is not restricted to the weak coupling case. Hence, as a general rule, we expect that in an isotropic sample the DDI tend to reduce the magnetization. However, this reasoning does not hold at high fields where the Zeeman term dominates on the DDI and where we expect an approach to saturation, close to what is obtained in the non interacting case deduced from the high field expansion of $M_r^{(0)}$ of equation (12), namely $(M_r(h) \sim 1 - 1/(\beta^* d_3^* h))$.

B. Spherical clusters in the strong coupling case

We now consider, exclusively for spherical clusters, the moderate to strong dipolar coupling case corresponding to the experimental situation of typical coated maghemite NP powders [24], with $\epsilon_d^{(0)} = 1$ for $d_{ref} = 10nm$ and a coating layer of $\Delta = 2.0nm$. The median diameter varies from d_{ref} to $2 \times d_{ref}$ and the standard deviation of the distribution $ln(d)$ is taken from $\sigma = 0.05$ to represent the quasi monodisperse case to $\sigma = 0.50$ to represent a large polydispersity. The importance of σ on the MNP distribution in the clusters is clearly seen on figure (2). Notice that a standard value obtained experimentally is *ca.* $0.20 \sim 0.30$ which is represented here by $\sigma = 0.28$. In the first step we neglect the anisotropy contribution ($\epsilon_K = 0$) and focus only on the DDI. First of all we analyse the linear susceptibility, χ which provides the behavior at low field of the magnetization. Since in our model, with a constant coating layer thickness, Δ, the dipolar coupling

constant scales as $(d_m/d_{ref})^3$ we expect in the vicinity of $h \sim 0$ a reduction of the magnetization higher for large median diameters, where the initial non interacting magnetization $M_r^{(0)}$ is higher. In the quasi monodisperse case, $\sigma = 0.05$ we make use of the scaling transformation introduced in equation (5) to explicit the effect of the coating layer thickness Δ on χ by using only one set of simulations for $\Delta/d_{ref} = 0.20$. We checked for $\Delta = 0.8$ and 2 values of d_m the reliability of this scaling transformation (see figure (4)). Therefore, in the quasi monodisperse case we have a rather complete picture of both the effect of the variation of the median diameter, d_m and of the distance of closest approach between NP, controlled by the coating layer thickness, Δ. The result for χ determined with $\sigma = 0.05$ is displayed and compared to the non interacting case $\chi^{(0)}$ in figure (4). As expected, when increasing the particle size and consequently the DDI coupling constant ϵ_d, an increasing reduction of χ is obtained. This reduction is of course all the more important that Δ is small. The important result is that we can get a plateau, which means that χ may becomes particle size independent beyond a threshold value which is, as expected, strongly Δ dependent. As already mentioned, for random distribution of easy axes, χ does not depend on ϵ_K in the superparamagnetic regime, and accordingly this result holds also in the case where the anisotropy is included.

The dependence of χ on both d_m and Δ can be used to deduce the behavior of χ with the NP volumic fraction (or concentration) at fixed value of d_m through the relation $\varphi_v = \varphi_m(d_m/(d_m + \Delta))^3$ with $\varphi_m = \varphi_v(\Delta = 0)$. Doing this, in agreement with other MC results [22, 39], we get a monotonous decrease of χ with the increase in φ, as shown on figure (5). Furthermore this shows that a fit of the NP size on the magnetization curve by using a Langevin function does not hold beyond a critical value φ_c of the volumic fraction. We can estimate this latter by imposing that $\chi/\chi(\epsilon_d = 0)$ is larger than some threshold value say λ, leading the determination of φ_c through $\chi(\varphi_c)/\chi(\epsilon_d = 0) = \lambda$. The result obtained by using $\lambda = 0.80$ is displayed on figure (5).

The magnetization curves in terms of the reduced external field H_a/H_{ref} for three values of the median diameter, still for $\sigma = 0.05$ is shown in figure (6) and compared to the non interacting diameter distribution weighted Langevin curves. We clearly see the important reduction of the magnetization compared to the non interacting case, and the very weak dependence of the low field behavior with respect to the median diameter which is expected as the considered sizes are either close to the onset of the $\chi(d_m)$ curve plateau corresponding to $(\Delta/d_{ref}) = 0.20$ ($d_m/d_{ref} = 1$) or pertain to this later ($d_m/d_{ref} = 1.33$ and 2.00). On the other hand at low external fields the nearly size independence of the magnetization is correlated with a quasi linear behavior of $M_r(h)$ with respect to h, which seems coherent with the interaction fields distribution description [23].

Then we introduce the polydispersity at fixed values of d_m. First we consider the case d_m/d_{ref}

= 1.33, as an example of median diameter located in the plateau region of the $\chi(d_m)$ curve. In this case we expect a very weak dependence of the magnetization with respect to the polydispersity in the low field region and this is confirmed by the MC simulations. Indeed, we get only small changes of $M_r(h)$ with σ as can be seen in figure (7). The magnetization curves corresponding to σ up to 0.40 are very close to each other for the values of the field for which $M_r < 0.70$; beyond this value, the deviations between the different magnetization curves reflect mainly the approach to saturation where $M_r(h) \sim (1 - 1/(\beta^* d_3^* h))$ depends on σ through d_3^*. The deviation from the quasi monodisperse situation over the whole field range occurs for $\sigma \geq 0.5$. Conversely, when the median diameter is taken outside of the $\chi(d_m)$ plateau, as is the case for $d_m/d_{ref} = 1.0$ the polydispersity has a noticeable influence on the magnetization as shown in figure (8) for σ ranging from 0.05 to 0.40.

In the superparamagnetic regime the MNP anisotropy energy modifies the magnetization curve for intermediate values of the field and leads to a reduction of M_r since the moments tend to be pinned in the easy axes directions. Taking into account ϵ_K thus reduces further M_r for h between the low field region controlled by the DDI and the approach to saturation controlled by the Zeeman energy. In the quasi monodisperse case, the blocking temperature corresponds to that of the median diameter, namely for non interacting particles, $k_B T_b \simeq K_1 v(d_m)/25$ or equivalently for the reduced blocking temperature $1/\beta_b^* \simeq \epsilon_K^{(0)}(d_m/d_{ref})^3/25$ leading to $1/\beta_b^* \simeq$ 0.225 for $d_m/d_{ref} = 1.33$. Here we restrict to the room temperature, $\beta^* = 1$, and we expect the system to be in the superparamagnetic regime even for short times. Indeed for $\sigma = 0.05$ our MC simulations confirm the superparamagnetic regime. The result is displayed and compared to the $\epsilon_K = 0$ case in figure (9) for $d_m/d_{ref} = 1.0$ and 1.33. As expected, the anisotropy energy does not affect the $M(H)$ curve in the vicinity of $H = 0$ due to the random distribution of easy axes. Moreover, when $d_m/d_{ref} = 1$, the $M(H)$ curve for intermediate values of the field is only weakly modified by the anisotropy energy while for $d_m/d_{ref} = 1.33$ a noticeable deviation is obtained.

The influence of the polydispersity on the magnetization curve when the anisotropy energy is included is shown for $d_m/d_{ref} = 1.33$ on figure (10) for σ ranging from 0.05 to 0.35. Because of the largest particles in the distribution, the system is no more in the superparamagnetic regime for the MC runs considered up to 10^5 MC steps. On the qualitative point of view this is expected since $1/\beta_b^*$ behaves as d^{*3} in the absence of DDI and moreover increases with the DDI. As a result an opening of the hysteresis cycle is obtained with remanence magnetization and coercive field increasing with σ as shown in figure (10) in the particular case $d_m/d_{ref} = 1.33$. The magnitude of the hysteresis cycle opening is expected to increase with d_m/d_{ref} and is indeed found very weak for $d_m/d_{ref} = 1.0$. The determination of the remanence in terms of d_m and the measuring time

is beyond the scope of this work; we nevertheless note (see section III C) that the hysteresis cycle opening for large values of d_m is in qualitative agreement with experiment.

C. Comparison with experiment

We now consider experimental results obtained recently on $\gamma - Fe_2O_3$ NP powders samples differing by their size [24]. The experimental protocol for the synthesis is described in [24]. The particles are coated with (5-hydroxy-5,5-bis(phosphono)pentanoic acid) which provides a coating layer of thickness ca 2 nm between particles. As a result of the synthesis method, the standard deviation of the diameter distributions as determined by TEM takes nearly the same value in the 4 samples considered, namely, $\sigma \simeq 0.26$. The saturation magnetization M_s is found to be in between 61 and 70 emu/g for the distributions characterized by $d_m = 10, 12, 18$ and 21 nm. Although these values are smaller than the bulk value at room temperature (~ 75 emu/g) the difference is small enough for the spin canting to be neglected in first approximation. It is worth mentioning that the magnetic properties of these NP assemblies have been measured also in diluted solution and, although the possible formation of clusters and/or chains in the presence of the external field cannot be ruled out, this allows for an estimation of the interaction effect. When going from the dispersed samples to the powder ones, we observe both a strong reduction of the magnetization and its weak size dependence in the low field region [24]. According to our simulations, both effects result from the DDI. The DDI induced reduction of $M_r(H)$ in the absence of demagnetizing effects is a general simulation result [22, 39, 40] and a similar trend has been obtained experimentally [41], and can be deduced from the FC/ZFC measurements in the superparamagnetic regime of either bare or Si coated $\gamma-Fe_2O_3$ NP [33]. Beside its rather weak size dependence the other feature of the experimental reduced magnetization curves, $M_r(H)$ in the low field region (see figure (11) is the opening of the hysteresis cycle for the largest sizes beyond $d_m = 12$ nm. These two points are in qualitative agreement with the MC simulations on our model although the opening of the cycle becomes noticeable for larger median diameters ($d_m \sim 18$ nm) than in MC simulations.

In the present work, we do not compare the experimental magnetization curve in the whole range of field with the results of either a mean field approach or the TPT. In any case the values of the dipolar coupling corresponding to the experimental powders samples ($\epsilon_d^{(eff)} \sim 0.6$ to 6.0 when $\epsilon_d \sim 1$ to 8 and the effect of Δ is taken into account) fall outside of the range of validity of the TPT. Indeed this later is limited to ca $\epsilon_d < 1/6$ according to ref. [20], the analytical approach based on TPT of ref. [18] is shown to be very accurate for $\epsilon_d < 0.25$ and valid for $\epsilon_d < 0.50$ in the monodisperse case and in section III A we found that χ as calculated from the TPT start to deviate from the simulated results at $\epsilon_d \sim 0.2$. Moreover the accounting of the polydispersity is

expected to worsen the lack of accuracy of the TPT with the increase of ϵ_d.

In figure (12) we compare the experimental and simulated $M_r(H)$ for the applied field in the low to intermediate range for $d_m = 10\ nm$. The agreement is quite satisfactory up to $H = 60$ kA/m where $M_r \simeq 0.7$. Then for median diameters $d_m > 12$ nm ($d_m/d_{ref} > 1.2$, we get for both the experimental samples and the MC simulations an opening of the hysteresis cycle. However, as can be deduced from figures (11) and (10) the irreversible field, H_{irr} is found much larger in the MC simulations than in the experiment. Notice that we do not try to map rigorously the MC time scale to the actual measurement time τ_m, and this is plays a central role on this point. Therefore concerning the MC simulations we consider in the following the anhysteretic magnetization as defined in equation (10); using this later remains to ignore the hysteresis cycle (*i.e.* the remanence and the coercive field) or to consider the infinite time scale limit. We compare the experimental $M(H)$ to the simulated ones in figures (13, 14) for the median sizes d_m 12 and 20 nm respectively. Given the simplicity of the model which does not include at all any structure in the particles, and the absence of fitting parameter the agreement is qualitatively satisfactory when $\epsilon_K^{(0)} = 2.38$ in particular for the overall variation of $M_r(H)$ at low fields ($H < 40$ kA/m).

Since in this range of fields, the deviation of M_r from the non interacting case is governed by the DDI, we can conclude that the strong reduction of the $M_r(H)$ variation with respect to H and its relative size independence when compared to the diluted solutions counterpart is the DDI signature. For median sizes larger than $d_m = 10\ nm$, the main discrepancy between the simulated and experimental $M_r(H)$ curves is the strong non linearity in the very vicinity of $H = 0$. This is clearly due to the oversimplification of the model in which the particles are uniform single domain ones.

D. Conclusion

In this work we have used MC simulations to investigate both the median size and polydispersity effects on the magnetization curve of densely packed clusters of single domain magnetic NP. An important result is the plateau in the $\chi(d_m)$ curve in the quasi monodisperse case for small values of the coating layer Δ, which emphasizes the much reduced size dependence of the $M(H)$ low field dependence in the concentrated systems. Despite of the simplicity of the model, some important features of the experimental $M(H)$ on powder samples are reproduced, especially concerning the DDI signature which occurs principally at low fields and its dependence on the particle size. In order to get a satisfactory agreement with experiments, it appears that the internal polarization structure of the NP should be introduced.

Acknowledgements

Tables

struct.	cs[a]	cfc[b]	rand. $\sigma = 0$ [c]	rand. $\sigma = 0.28$ [d]
φ_v	$\pi/6$	0.74	0.525	0.580
$C_2^{(f)}$	0.2775	0.3367	0.2534	1.7934
$C_2^{(g)}$	-0.4745	-0.6109	-0.4390	-3.1506
$C_2^{(h)}$	0.2217	0.3133	0.2217	1.6173
$C_2^{(i)}$	-0.4433	-0.6265	-0.4433	-3.2354

Table I: Second derivative $C_2 = \partial^2(\Delta M_r)/\partial \epsilon_d \partial h$ at $\epsilon_d = 0$ and $h = 0$ for a primatic cluster of $1024^{(a)}$, $1103^{(b)}$, $1054^{(c)}$ and $879^{(d)}$ particles, characterized by $L_x = L_y$ and $L_z = L_x/5$. MC simulation with $\hat{h} = \hat{x}$ [f], $\hat{h} = \hat{z}$ [g]; equation (18) with $\hat{h} = \hat{x}$ [h], $\hat{h} = \hat{z}$ [i]. [h], [i] The demagnetizing factor entering equation (18) is taken from [42] and the moments d_s^* are taken from the actual diameters distribution of the cluster considered.

[1] J. L. Dormann, D. Fiorani, and E. Tronc, "Advances in chemical physics," (John Wiley and Sons, Inc., 1997) pp. 283–494.

[2] R. Skomski, J. Phys.: Condens. Matter **15**, R841 (2003).

[3] S. Majetich and M. Sachan, J. Phys D **39**, R407 (2006).

[4] S. Bedanta and W. Kleemann, J. Phys D **42**, 013001 (2009).

[5] Y. Lalatonne, L. Motte, J. Richardi, and M. P. Pileni, Phys. Rev. E **71**, 011404 (2005).

[6] Y. Lalatonne, C. Paris, J. M. Serfaty, P. Weinmann, M. Lecouvey, and L. Motte, Chem. Commun. , 2553 (2008).

[7] Y. Lalatonne, L. Motte, V. Russier, A. T. Ngo, P. Bonville, and M. P. Pileni, The Journal of Physical Chemistry B **108**, 1848 (2004).

[8] J. M. D. Coey, Phys. Rev. Lett. **27**, 1140 (1971).

[9] E. Tronc, A. Ezzir, R. Cherkaoui, C. Chanéac, M. Noguès, H. Kachkachi, D. Fiorani, A. Testa, J. Grenèche, and J. Jolivet, Journal of Magnetism and Magnetic Materials **221**, 63 (2000).

[10] E. Tronc, D. Fiorani, M. Noguès, A. Testa, F. Lucari, F. D'Orazio, J. Grenèche, W. Wernsdorfer, N. Galvez, C. Chanéac, D. Mailly, and J. Jolivet, Journal of Magnetism and Magnetic Materials **262**, 6 (2003).

[11] X. Battle and A. Labarta, J. Phys D **35**, R15 (2002).

[12] M. P. Morales, S. Veintemillas-Verdaguer, M. I. Montero, C. J. S erna, A. Roig, L. Casas, B. Martínez, and F. Sandiumenge, Chemistry of Materials **11**, 3058 (1999).

[13] J.-P. Fortin, C. Wilhelm, J. Servais, C. Ménager, J.-C. Bacri, and F. Gazeau, Journal of the American Chemical Society **129**, 2628 (2007).

[14] D.-X. Chen, A. Sanchez, E. Taboada, A. Roig, N. Sun, and H.-C. Gu, Journal of Applied Physics **105**, 083924 (2009).

[15] J. García-Palacios, "Advances in chemical physics," (John Wiley and Sons, Inc., 2000) pp. 1–210.

[16] F. Wiekhorst, E. Shevchenko, H. Weller, and J. Kötzler, Phys. Rev. B **67**, 224416 (2003).

[17] R. Yanes, O. Chubykalo-Fesenko, H. Kachkachi, D. A. Garanin, R. Evans, and R. W. Chantrell, Phys. Rev. B **76**, 064416 (2007).

[18] G. Margaris, K. Trohidou, and H. Kachkachi, Phys. Rev. B **85**, 024419 (2012).

[19] H. Kachkachi and E. Bonet, Phys. Rev. B **73**, 224402 (2006).

[20] P. E. Jönsson and J. L. García-Palacios, Phys. Rev. B **64**, 174416 (2001).

[21] D. Kechrakos and K. N. Trohidou, Phys. Rev. B **62**, 3941 (2000).

[22] R. W. Chantrell, N. Walmsley, J. Gore, and M. Maylin, Phys. Rev. B **63**, 024410 (2000).

[23] J. Al-Saei, M. El-Hilo, and R. W. Chantrell, Journal of Applied Physics **110**, 023902 (2011).

[24] C. de Montferrand, Y. Lalatonne, D. Bonnin, N. Lièvre, M. Lecouvey, P. Monod, V. Russier, and L. Motte, Small **8**, 1945 (2012) .

[25] J. L. García-Palacios, P. Jönsson, and P. Svedlindh, Phys. Rev. B **61**, 6726 (2000).

[26] H. Kachkachi and M. Azeggagh, Eur. Phys. J. B **44**, 299 (2005).

[27] E. du Trémolet de Lacheisserie, "Magnétisme," (EDP Sciences, 2000) in french.

[28] J. M. D. Coey, "Magnetism and magnetic materials," (Cambridge University Press, 2010).

[29] W. Soppe, Powder Technology **62**, 189 (1990).

[30] F. Gazeau, J. Bacri, F. Gendron, R. Perzynski, Y. Raikher, V. Stepanov, and E. Dubois, Journal of Magnetism and Magnetic Materials **186**, 175 (1998).

[31] D. Fiorani, A. M. Testa, F. Lucari, F. D'Orazio, and H. Romero, Physica B **320**, 122 (2002).

[32] G. C. Papaefthymiou, E. Devlin, A. Simopoulos, D. K. Yi, S. N. Riduan, S. S. Lee, and J. Y. Ying, Phys. Rev. B **80**, 024406 (2009).

[33] C. Pereira, A. M. Pereira, P. Quaresma, P. B. Tavares, E. Pereira, J. P. Araujo, and C. Freire, Dalton Trans. **39**, 2842 (2010).

[34] M. Levy, A. Quarta, A. Espinosa, A. Figuerola, C. Wilhelm, M. García-Hernández, A. Genovese, A. Falqui, D. Alloyeau, R. Buonsanti, P. D. Cozzoli, M. A. García, F. Gazeau, and T. Pellegrino, Chemistry of Materials **23**, 4170 (2011).

[35] K. Binder and D. W. Heerman, "Monte carlo simulation in statistical physics," (Springer, 1997).

[36] M. P. Allen and D. J. Tildesley, "Computer simulation of liquids," (Oxford Science Publications, 1987).

[37] U. Nowak, R. W. Chantrell, and E. C. Kennedy, Phys. Rev. Lett. **84**, 163 (2000).

[38] X. Z. Cheng, M. B. A. Jalil, H. K. Lee, and Y. Okabe, Phys. Rev. Lett. **96**, 067208 (2006).

[39] D. Serantes, D. Baldomir, C. Martinez-Boubeta, K. Simeonidis, M. Angelakeris, E. Natividad, M. Castro, A. Mediano, D.-X. Chen, A. Sanchez, L. Balcells, and B. Martínez, Journal of Applied Physics **108**, 073918 (2010).

[40] J. García-Otero, M. Porto, J. Rivas, and A. Bunde, Phys. Rev. Lett. **84**, 167 (2000).

[41] M. Gonzales-Weimuller, M. Zeisberger, and K. M. Krishnan, Journal of Magnetism and Magnetic Materials **321**, 1947 (2009).

[42] A. Aharoni, Journal of Applied Physics **83**, 3432 (1998).

Figure captions

Figure 1 Shematic view of the configuration for two particles coated by the layer of thickness $\Delta/2$ at contact.

Figure 2 Central part of the clusters corresponding to $d_m/d_{ref} = 1.33$ and $\sigma = 0.05$, 0.28 and 0.50 from top to bottom.

Figure 3 Comparison of χ_r in terms of ϵ_d as calculated from the TPT of Ref. [15], (solid line) and the present MC simulation (symbols) for a spherical cluster of simple cubic structure with $N_p = 1021$ particles and a monodisperse distribution. $\beta^* = 1.0$.

Figure 4 Linear susceptibility in terms of the median size d_m/d_{ref} for different values of the coating layer thickness Δ in the quasi monodisperse case, $\sigma = 0.05$ and $\beta^* = 1.0$. The two crosses on the $\Delta/d_{ref} = 0.8$ curve correspond to the direct calculation without using the scaling transformation (6). The dotted lines are guides to the eye and the solid line corresponds to the non interacting case.

Figure 5 Susceptibility χ in terms of the reduced volumic fraction, for $\sigma = 0.05$, $\beta^* = 1.0$, and d_m/d_{ref} = 2.0 (solid circles); 1.50 (solid squares); 1.25 (upward triangles) and 1.0 (downward triangles). $\varphi_m = \varphi(\Delta = 0)$. In the present work $\varphi_m \simeq 0.585$. Inset: reduced critical volumic fraction defined as $\chi(\varphi, \epsilon_d)/\chi(\epsilon_d = 0) = 0.80$ in terms of the median particle size.

Figure 6 Magnetization in terms of the applied field for different values of the median diameter, Δ/d_{ref} = 0.20, $\beta^* = 1.0$ and $N_p = 1007$ in the quasi monodisperse case, $\sigma = 0.05$. The corresponding non interacting curves (diameter distribution weighted Langevin curves) for $d_m/d_{ref} = 1.0$ (long dash), 1.33 (short dash) and 2.0 (dotted line) are displayed for comparison.

Figure 7 Magnetization in terms of the applied field for different values of the $ln(d)$ standard deviation σ and $d_m/d_{ref} = 1.33$, $\Delta/d_{ref} = 0.20$ and $\beta^* = 1.0$. $N_p = 1007$ ($\sigma = 0.05$), 923 ($\sigma = 0.28$); 985 ($\sigma = 0.40$) and 990 ($\sigma = 0.50$). The dotted lines are quides to the eye. The solid lines are the asymptotic limits for $\sigma = 0.05$ (bottom) and $\sigma = 0.50$ (top).

Figure 8 Magnetization in terms of the applied field for $\sigma = 0.05$, 0.20, 0.28 and 0.40 from bottom to top. and $d_m/d_{ref} = 1.00$, $\Delta/d_{ref} = 0.20$, $\beta^* = 1.0$. The dotted lines are guides to the eyes and the solid lines are the corresponding asymptotic limits for $\sigma = 0.05$ and $\sigma = 0.40$.

Figure 9 Magnetization curve with the anisotropy energy $\epsilon_K^{(0)} = 2.38$, $\sigma = 0.05$ and the particles sizes as indicated. The solid lines correspond to $\epsilon_K = 0$. $\beta^* = 1$ and $N_p = 1007$.

Figure 10 Magnetization curve with the anisotropy energy $\epsilon_K^{(0)} = 2.38$, $d_m/d_{ref} = 1.33$ and $\beta^* = 1$ in the polydisperse case with $\sigma = 0.35$ (open circles); 0.28 (triangles); 0.20 (squares) compared to the quasi monodisperse case, $\sigma = 0.05$ (solid line). Insert: detail of the downward magnetization curve in the vicinity of $h = 0$, showing the evolution of the remanence and coercivity with σ for $\sigma = 0.35$, 0.28, 0.20 and 0.10 (open squares) from top to bottom.

Figure 11 Experimental low field magnetization curves at room temperature for powder samples of $\gamma - Fe_2O_3$ from ref. [24] with polydispersity $\sigma \simeq 0.26$ and median sizes as indicated.

Figure 12 Comparison between MC simulations and the experimental magnetization curve at room temperature for $d_m = 10\ nm$. The simulation are performed with $\beta^* = 1$, $\epsilon_K^{(0)} = 2.38$ and $N_p = 923$.

Figure 13 Comparison between MC simulations and the experimental magnetization curve at room temperature for $d_m = 12\ nm$. The simulations are performed with $\beta^* = 1$, $N_p = 980$, $\epsilon_K^{(0)} = 2.38$ (open circles) or 1.19 (dashed line). The dooted line is a guide to the eye.

Figure 14 Comparison between MC simulations and the experimental magnetization curve at room temperature for $d_m = 21\ nm$. The simulations are performed with $d_m = 20$ nm, $\beta^* = 1$, $N_p = 998$, $\epsilon_K^{(0)} = 2.38$ (open circles) or 1.19 (dashed line).
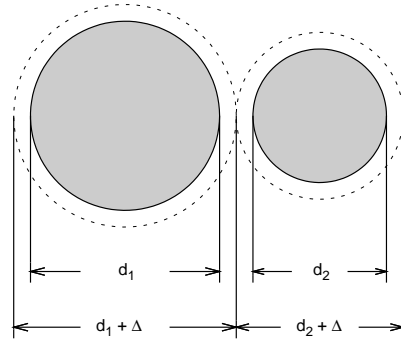
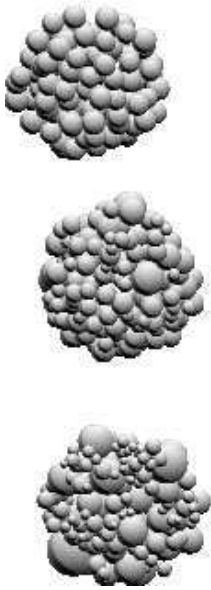Figure 1: Shematic view of the configuration for two particles coated by the layer of thickness $\Delta/2$ at contact.

Figure 2: Central part of the clusters corresponding to $d_m/d_{ref} = 1.33$ and $\sigma = 0.05$, 0.28 and 0.50 from top to bottom.
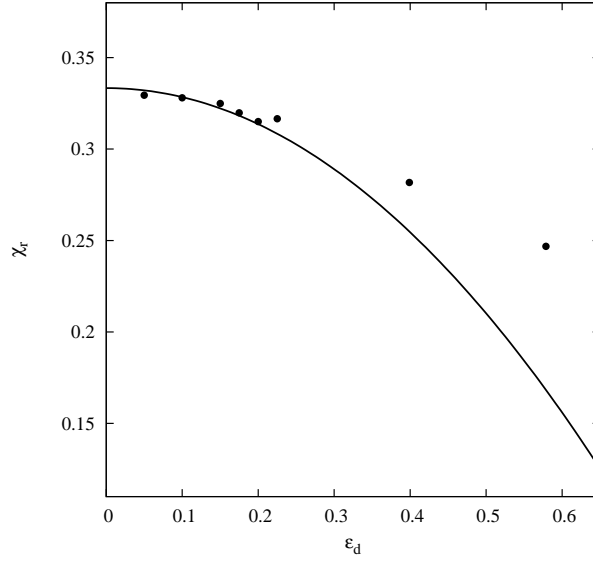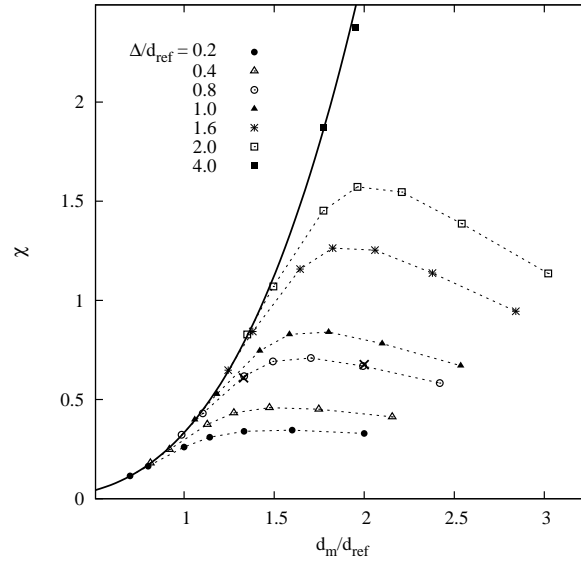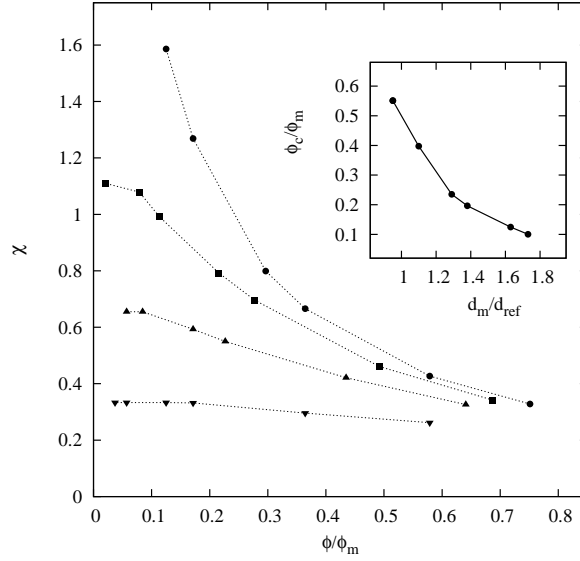
Figure 3: Comparison of χ_r in terms of ϵ_d as calculated from the TPT of Ref. [15], (solid line) and the present MC simulation (symbols) for a spherical cluster of simple cubic structure with $N_p = 1021$ particles and a monodisperse distribution. $\beta^* = 1.0$.

Figure 4: Linear susceptibility in terms of the median size d_m/d_{ref} for different values of the coating layer thickness Δ in the quasi monodisperse case, $\sigma = 0.05$ and $\beta^* = 1.0$. The two crosses on the $\Delta/d_{ref} = 0.8$ curve correspond to the direct calculation without using the scaling transformation (6). The dotted lines are guides to the eye and the solid line corresponds to the non interacting case.

Figure 5: Susceptibility χ in terms of the reduced volumic fraction, for $\sigma = 0.05$, $\beta^* = 1.0$, and d_m/d_{ref} = 2.0 (solid circles); 1.50 (solid squares); 1.25 (upward triangles) and 1.0 (downward triangles). $\varphi_m = \varphi(\Delta = 0)$. In the present work $\varphi_m \simeq 0.59$. Inset: reduced critical volumic fraction defined as $\chi(\varphi, \epsilon_d)/\chi(\epsilon_d = 0) = 0.80$ in terms of the median particle size.
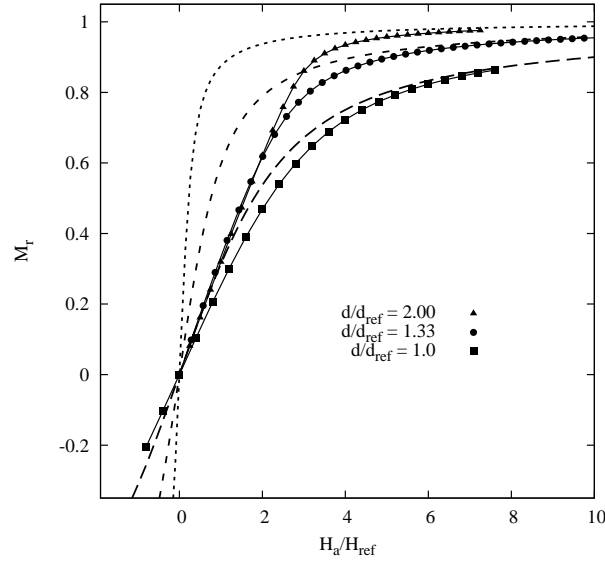
Figure 6: Magnetization in terms of the applied field for different values of the median diameter, $\Delta/d_{ref} = 0.20$, $\beta^* = 1.0$ and $N_p = 1007$ in the quasi monodisperse case, $\sigma = 0.05$. The corresponding non interacting curves (diameter distribution weighted Langevin curves) for $d_m/d_{ref} = 1.0$ (long dash), 1.33 (short dash) and 2.0 (dotted line) are displayed for comparison.

Figure 7: Magnetization in terms of the applied field for different values of the $ln(d)$ standard deviation σ and $d_m/d_{ref} = 1.33$, $\Delta/d_{ref} = 0.20$ and $\beta^* = 1.0$. $N_p = 1007$ ($\sigma = 0.05$), 923 ($\sigma = 0.28$); 985 ($\sigma = 0.40$) and 990 ($\sigma = 0.50$). The dotted lines are quides to the eye. The solid lines are the asymptotic limits for σ = 0.05 (bottom) and $\sigma = 0.50$ (top).
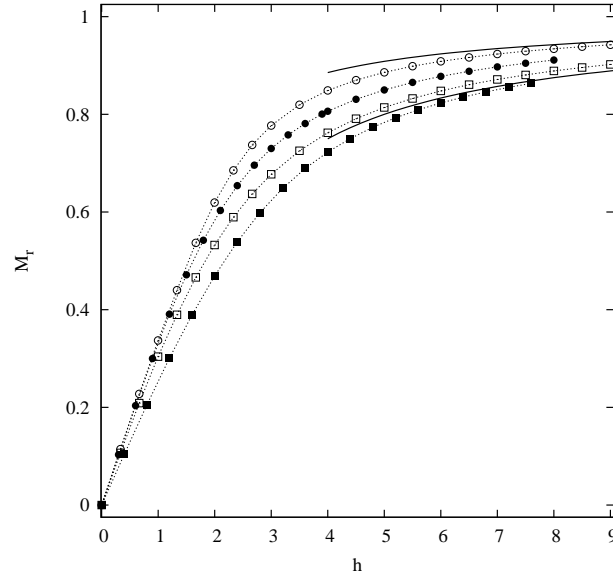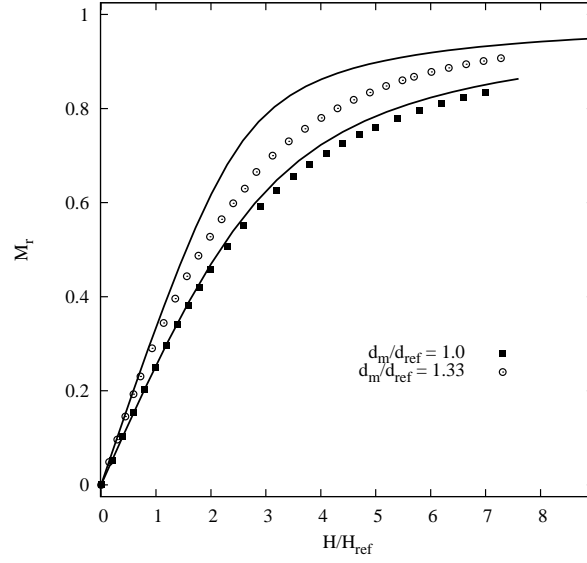

Figure 8: Magnetization in terms of the applied field for $\sigma = 0.05$, 0.20, 0.28 and 0.40 from bottom to top. and $d_m/d_{ref} = 1.00$, $\Delta/d_{ref} = 0.20$, $\beta^* = 1.0$. The dotted lines are guides to the eyes and the solid lines are the corresponding asymptotic limits for $\sigma = 0.05$ and $\sigma = 0.40$.

Figure 9: Magnetization curve with the anisotropy energy $\epsilon_K^{(0)} = 2.38$, $\sigma = 0.05$ and the particles sizes as indicated. The solid lines correspond to $\epsilon_K = 0$. $\beta^* = 1$ and $N_p = 1007$.
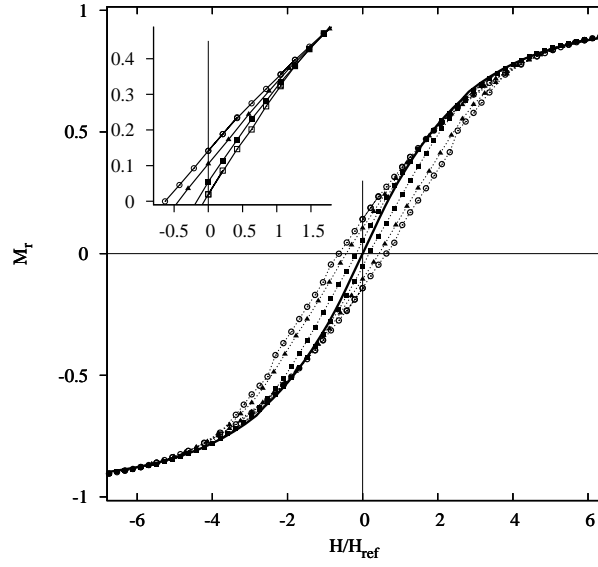

Figure 10: Magnetization curve with the anisotropy energy $\epsilon_K^{(0)} = 2.38$, $d_m/d_{ref} = 1.33$ and $\beta^* = 1$ in the polydisperse case with $\sigma = 0.35$ (open circles); 0.28 (triangles); 0.20 (squares) compared to the quasi monodisperse case, $\sigma = 0.05$ (solid line). Insert: detail of the downward magnetization curve in the vicinity of $h = 0$, showing the evolution of the remanence and coercivity with σ for $\sigma = 0.35$, 0.28, 0.20 and 0.10 (open squares) from top to bottom.
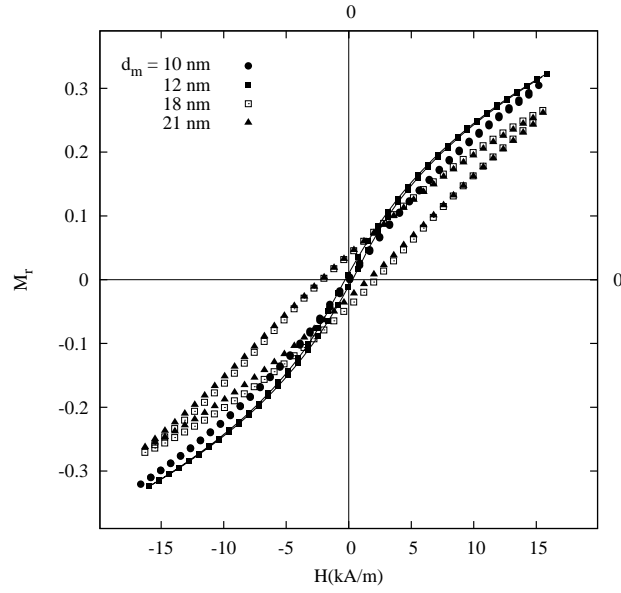
Figure 11: Experimental low field magnetization curves at room temperature for powder samples of $\gamma-Fe_2O_3$ from ref. [24] with polydispersity $\sigma \simeq 0.26$ and median sizes as indicated.
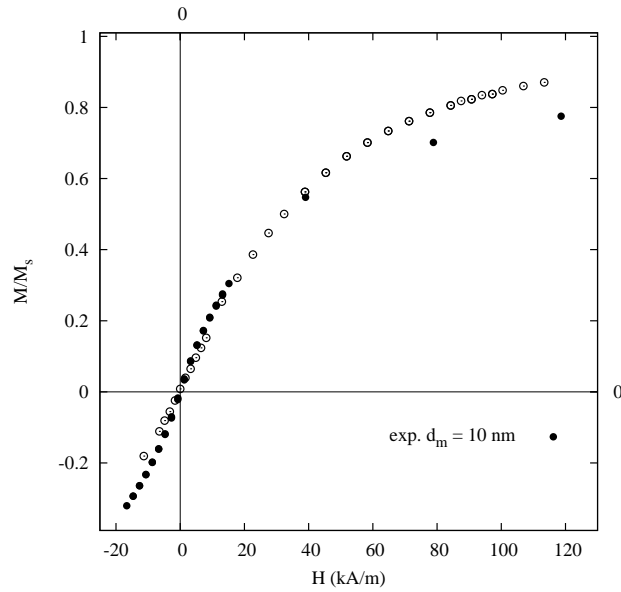

Figure 12: Comparison between MC simulations and the experimental magnetization curve at room temperature for $d_m = 10 \ nm$. The simulation are performed with $\beta^* = 1$, $\epsilon_K^{(0)} = 2.38$ and $N_p = 923$.
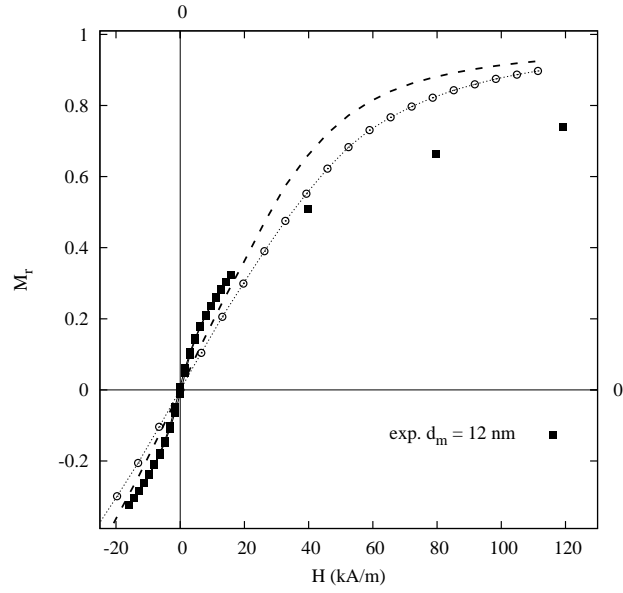
Figure 13: Comparison between MC simulations and the experimental magnetization curve at room temperature for $d_m = 12\ nm$. The simulations are performed with $\beta^* = 1$, $N_p = 980$, $\epsilon_K^{(0)} = 2.38$ (open circles) or 1.19 (dashed line). The dooted line is a guide to the eye.
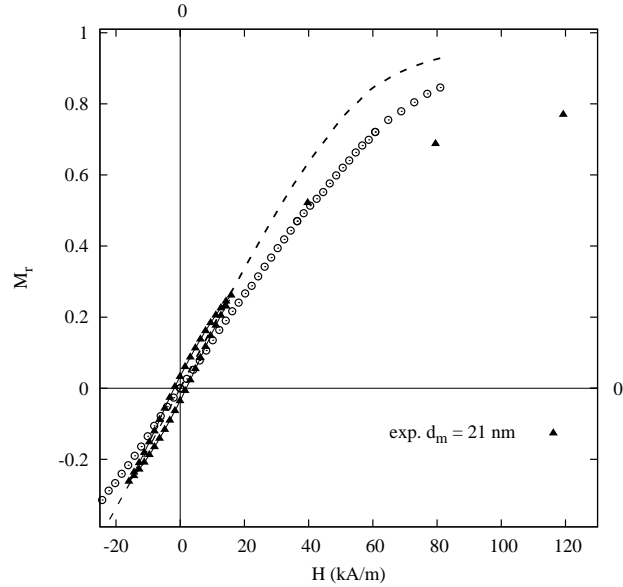

Figure 14: Comparison between MC simulations and the experimental magnetization curve at room temperature for $d_m = 21\ nm$. The simulations are performed with $d_m = 20$ nm, $\beta^* = 1$, $N_p = 998$, $\epsilon_K^{(0)} = 2.38$ (open circles) or 1.19 (dashed line).